IOP Publishing Journal of Physics: Condensed Matter
J. Phys.: Condens. Matter **32** (2020) 174002 (9pp) https://doi.org/10.1088/1361-648X/ab6b8f

Origin of the phase separation into B2 and $L2_1$ ordered phases in X–Al–Ti (X: Fe, Co, and Ni) alloys based on the first-principles cluster variation method

Ryo Yamada[1] **and Tetsuo Mohri**[2]

[1] Division of Materials and Manufacturing Science, Graduate School of Engineering, Osaka University, Suita, Osaka 565-0871, Japan
[2] Institute for Materials Research, Tohoku University, Sendai 980-8577, Japan

E-mail: r-yamada@mat.eng.osaka-u.ac.jp and tmohri@imr.tohoku.ac.jp

Received 31 October 2019, revised 15 December 2019
Accepted for publication 14 January 2020
Published 28 January 2020

Abstract

The phase separation behaviors from a single B2 ordered phase into two separate B2 and $L2_1$ ordered phases in X–Al–Ti (X: Fe, Co, and Ni) alloys are analyzed utilizing the cluster variation method (CVM), based on interaction energies derived from electronic band structure calculations. A cubic approximation of the CVM is adopted for $X_2Al_{2-x}Ti_x$ ($0 \leqslant x \leqslant 2$) alloys limiting the interchange between Al and Ti atoms on the α- and β-sublattices of an $L2_1$ ordered structure with X atoms fixed on the γ-sublattice. The phase stabilities of the B2 and $L2_1$ structures are examined, and phase diagrams at the pseudo-binary section, XAl–XTi, are determined. The two-phase regions of the B2 and $L2_1$ phases (i.e. phase separation behavior) are successfully produced in Co– and Ni–Al–Ti alloy systems, and no phase separation is observed in the Fe–Al–Ti alloy. The origins of phase separation in the Co– and Ni–Al–Ti alloys are mechanical instability and a combination of mechanical instability and chemical repulsions of unlike pairs, respectively.

Keywords: cluster variation method, first-principles calculation, order-disorder phase transformation, mechanical instability, phase separation

(Some figures may appear in colour only in the online journal)

1. Introduction

The decomposition of a solid solution into two separate phases in metallic alloy systems is one of the most well-known and widely studied phenomena in materials science. In general, such decomposition is mechanically and/or chemically induced. When an initial solid solution becomes unstable or metastable in a given environment, such as an environment with high pressures and/or low temperatures, it decomposes into two different phases. This phenomenon is well-described by empirical rules known as the Hume–Rothery rules, where the following three factors are utilized to evaluate the phase stability of a single solid solution in an alloy system [1]: differences in atomic radii, electronegativity, and valence electron concentrations. Each of these factors is estimated from the constituent elements of the given alloy system. The first factor is related to mechanically driven phase separations, and the other two factors are related to chemically driven phase separations.

Mechanically induced phase separation originates from mechanical instability. Mechanical instability can be easily detected based on pressure–volume (P–V) curves. A P–V curve represents the second-order derivative of the energy (or free energy), E, in terms of volume, V, because $\partial^2 E/\partial V^2 = -\partial P/\partial V$. To be mechanically stable, a system must satisfy the condition $\partial P/\partial V < 0$ at an equilibrium volume, where the curve intersects with the horizontal axis (i.e. $P = P_{\mathrm{ext}} \approx 0$). The concept of mechanical instability

leading to the phase separation has been applied to liquid–gas transformations [2], but is also applicable to solid–solid transformations [3].

In contrast, chemically driven phase separation can be concisely described by a first-nearest-neighbor pair interaction model. For example, when the two components of an A–B alloy have stronger bonding for A–A and B–B pairs than for A–B (or B–A) pairs, the ground-state structure will be composed of two chemically distinct phases, namely A-rich and B-rich solid solutions. At relatively high temperatures, entropic contribution becomes dominant and a single solid solution (or disordered phase) will become more stable than two separate phases. Conversely, a high-temperature single solid solution can decompose into two different phases at low temperatures.

In some alloy systems, phase separation with accompanying ordering has been observed (e.g. [4–6]). This phenomenon is known as the concurrent behavior of ordering and phase separation. Concurrent behavior in Fe–Be alloys transitioning from a single solid solution into a solid solution and B2 ordered phase has been successfully explained by considering distant pair interactions [4]. It has been suggested that when first-nearest-neighbor interactions prefer ordering, but second-neighbors promote phase separation, there is the potential for concurrent behavior of ordering and phase separation [4, 7].

In Co– and Ni–Al–Ti ternary alloys, a phenomenon similar to the concurrent behavior mentioned above has been observed [8–10]. In these cases, a B2 ordered phase decomposes into B2 and $L2_1$ ordered phases. It is noteworthy that both B2 and $L2_1$ ordered phases have been observed in Fe–Al–Ti systems as well, but phase separation behavior has not been observed [8]. There have been several works suggesting that the phase separation in Ni–Al–Ti alloys is caused by a lattice misfit between B2 and $L2_1$ phases [11, 12] (i.e. caused by mechanical instability).

However, because the transformation between B2 and $L2_1$ phases in X–Al–Ti alloys can be viewed as an order–disorder phase transformation (because the $L2_1$ phase is crystallographically equivalent to the B2 phase when the Al and Ti atoms on the α- and β-sublattices are randomly distributed, as shown in figure 1(b)), the same reasoning applied to Fe–Be alloys [4] is also applicable to X–Al–Ti alloys. A systematic study was conducted on X–Al–Ti alloys to investigate effects of X (X: Fe, Co, Ni, and Cu) atoms on the stability of the two-phase region, and a specific relationship between phase separation and the numbers of $3d + 4s$ valence electrons in the component elements was proposed [10]. This indicates that phase separation into B2 and $L2_1$ ordered phases in X–Al–Ti alloys is strongly related to chemical affinities.

The origin of phase separation in X–Al–Ti alloys is still controversial and has not been fully elucidated. Therefore, in this study, the origins of phase separation in Co– and Ni–Al–Ti alloys, as well as the reason for its absence in Fe–Al–Ti alloys, were explored utilizing the cluster variation method (CVM) [13]. The CVM is one of the most reliable mean field approximations for formulating free energy. By combining it with electronic structure total energy calculations (first-principles CVM [14]), it is expected that the phase stability of B2 and $L2_1$ ordered structures can be reliably evaluated in terms of both mechanical instability and chemical repulsions of unlike pairs.

The remainder of this paper is organized as follows. The methodology for analysis of the phase stability of B2 and $L2_1$ ordered structures utilizing first-principles CVM is described in section 2. In Section 3, the calculated phase diagrams for X–Al–Ti (X: Fe, Co, and Ni) alloys in XAl–XTi pseudo-binary sections are presented and the contributions of mechanical instability and chemical repulsions are discussed. Finally, the origin of phase separation in X–Al–Ti alloys is summarized in section 4.

2. Theory

The phase stability of B2 and $L2_1$ ordered phases in Ni–Al–Ti alloys was analyzed based on CVM by Enomoto *et al* [12]. In their study, the phenomenological interaction energies between first- and second-nearest-neighbor pairs on an original body-centered cubic (bcc) lattice were utilized within tetrahedron approximation. The two-phase region of the B2 and $L2_1$ ordered phases was successfully predicted in a Ti-rich environment and phase separation behavior was explained in terms of large lattice misfits between B2 and $L2_1$ ordered phases without referring to the chemical affinities of atomic bonds in the system. In fact, to elucidate chemical contributions, it is necessary to consider longer interaction energies compared to second-nearest-neighbor pairs on the bcc lattice (which correspond to first-nearest-neighbor pairs on a simple cubic lattice, as shown in figure 1). Longer pair interaction energy cannot be considered in the tetrahedron approximation. Therefore, a higher-order approximation must be adopted to incorporate longer pair interaction energy. The next higher-order approximation for the bcc structure is the cube-octahedron approximation [15], but the cube-octahedron approximation is non-trivial because of its huge computational burden.

The phase stability of B2 and $L2_1$ ordered structures has also been explored in $X_2A_{2-x}B_x$ ($0 \leqslant x \leqslant 2$) alloys utilizing a cubic approximation of the CVM by Kiyokane [16], who only considered interchange between A and B atoms on the α- and β-sublattices of $L2_1$ ordered structures with fixed X atoms on the γ-sublattice (see figure 1, where A and B atoms correspond to Al and Ti atoms, respectively). The author conducted model calculations by setting an arbitrary constant value for the first-nearest-neighbor pair interaction energies on a simple cubic lattice (not the bcc lattice) and identified a phase boundary between B2 and $L2_1$ phases in the XA–XB pseudo-binary section. Because any volume dependence on pair interaction energies and any additional distant pair interaction energies beyond the first-nearest neighbors were not considered, a two-phase region ($B2 + L2_1$) was not produced. However, this scheme has an advantageous feature compared to the tetrahedron CVM employed by Enomoto *et al* [12] in that it is possible to include longer interaction energies than second-nearest-neighbor pairs on the bcc lattice

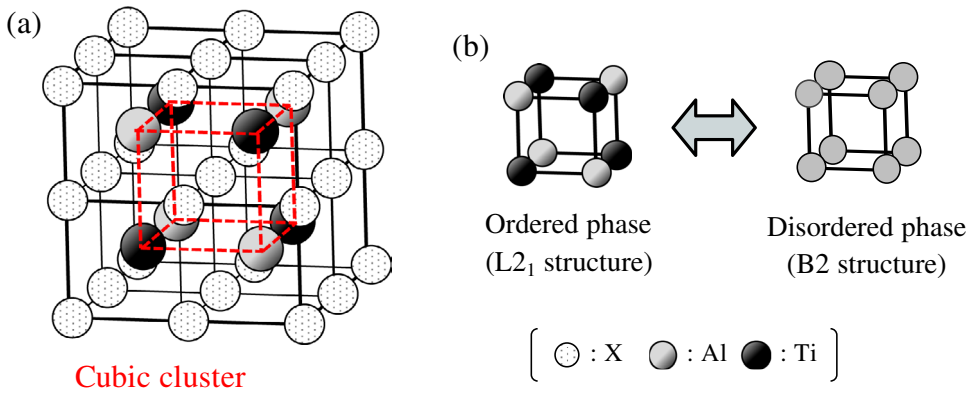

Figure 1. (a) $L2_1$ ordered structure, where X, Al, and Ti atoms are represented by dotted, gray, and black balls, respectively. Lattice points that are predominately occupied by Al, Ti, and X atoms are called the α-, β-, and γ-sublattices, respectively. (b) The $L2_1$ structure transforms into a B2 structure when the Al and Ti atoms are randomly distributed on the α- and β-sublattices, which can be viewed as an ordered–disordered phase transformation. The cubic cluster on the simple cubic lattice composed of α- and β-sublattices is highlighted in red. This cluster is utilized as the basic cluster for the cubic approximation of the CVM.

Table 1. Twenty-two types of cubic configurations, each of which is numbered with its interaction energies shown as ϵ_n.

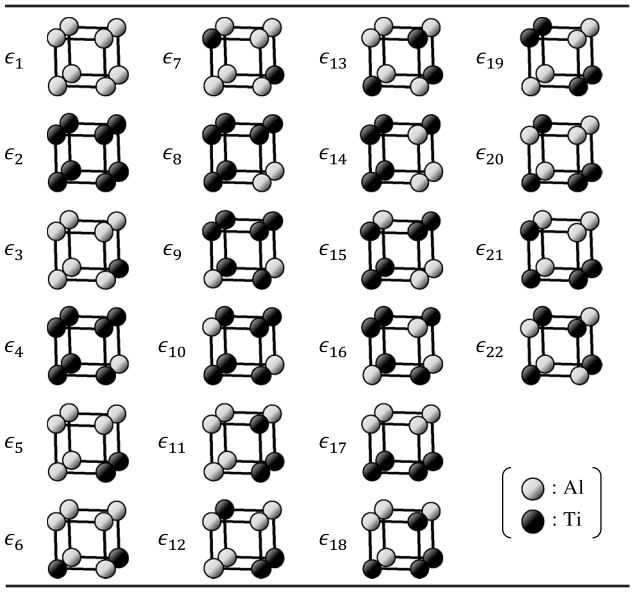

(or first-nearest-neighbor pairs on a simple cubic lattice) with a relatively small computational burden compared to the cube-octahedron approximation.

Therefore, in the calculations for this study, a cubic approximation of the CVM is implemented by considering multi-body interaction energies inside a cubic cluster (including up to the third-nearest-neighbor pair of interaction energies for the simple cubic lattice), which are determined through electronic band structure calculations. In the cubic approximation employed in this study, the only configurations of Al and Ti atoms on α- and β-sublattices are considered as was done in [16]. In the remainder of this section, the phase equilibria between the B2 and $L2_1$ ordered phases in the $X_2Al_{2-x}Ti_x$ ($0 \leqslant x \leqslant 2$) alloys are explored and phase diagrams for the pseudo-binary section, XAl–XTi, are determined.

Note that a concept similar to that adopted here (i.e. limiting one's attention to atomic configurations to the α- and β-sublattices) has been employed for the calculation of the tetragonal–cubic phase transformation in ZrO_2 [14, 17], where only the displacements of oxygen atoms were considered with fixed zirconium positions. Because there is clear (reliable) experimental evidence that the Fe, Co, and Ni atoms in X–Al–Ti alloys are located primarily on the γ-sublattice [8–10], the assumption adopted here is reasonable as long as the temperature is not excessively high.

For the analysis of phase stability, the free energy of a system must be formulated. The configurational entropy, S, within the cubic approximation of the CVM is given as [18]

$$S = k_{\mathrm{B}}\left[\frac{1}{2}\left(\sum_i L(x_i^{\alpha}) + \sum_i L(x_i^{\beta})\right) - 3\sum_{i,j} L(y_{ij}^{\alpha\beta}) + 3\sum_{i,j,k,l} L(z_{ijkl}^{\alpha\beta\alpha\beta}) - \sum_{i,j,k,l,m,n,o,p} L(w_{ijklmnop}^{\alpha\beta\alpha\beta\alpha\beta\alpha\beta})\right], \quad (1)$$

where k_{B} is the Boltzmann constant; $x_i^{\alpha/\beta}$, $y_{ij}^{\alpha\beta}$, $z_{ijkl}^{\alpha\beta\alpha\beta}$, and $w_{ijklmnop}^{\alpha\beta\alpha\beta\alpha\beta\alpha\beta}$ are the cluster probabilities of the point, pair, square, and cubic, respectively; and $L(x) \equiv x\ln x - x$. The subscripts and superscripts of the cluster probabilities indicate atomic species and sublattices, respectively (e.g. $z_{\mathrm{AlAlAlTi}}^{\alpha\beta\alpha\beta}$ represents the probability of finding the square configuration, namely Al–Al–Al–Ti, on the α-β-α-β sublattices).

The total energy, E, in a system is described in terms of cubic interaction energy as

$$E = \sum_{i,j,k,l,m,n,o,p} \epsilon_{ijklmnop} w_{ijklmnop}^{\alpha\beta\alpha\beta\alpha\beta\alpha\beta}, \quad (2)$$

where $\epsilon_{ijklmnop}$ are the cubic interaction energies and $w_{ijklmnop}^{\alpha\beta\alpha\beta\alpha\beta\alpha\beta}$ are the cubic cluster probabilities, as defined above. Although there are $2^8 = 256$ possible cubic configurations for Al and Ti atoms, this number is significantly reduced to 22 based on the symmetry of the cubic structure. The cubic configurations are numbered and listed in table 1. Note that the perfect B2 and $L2_1$ ordered phases (or XAl, XTi, and X_2AlTi) correspond to the first, second, and 22nd cubic configurations in table 1, respectively.

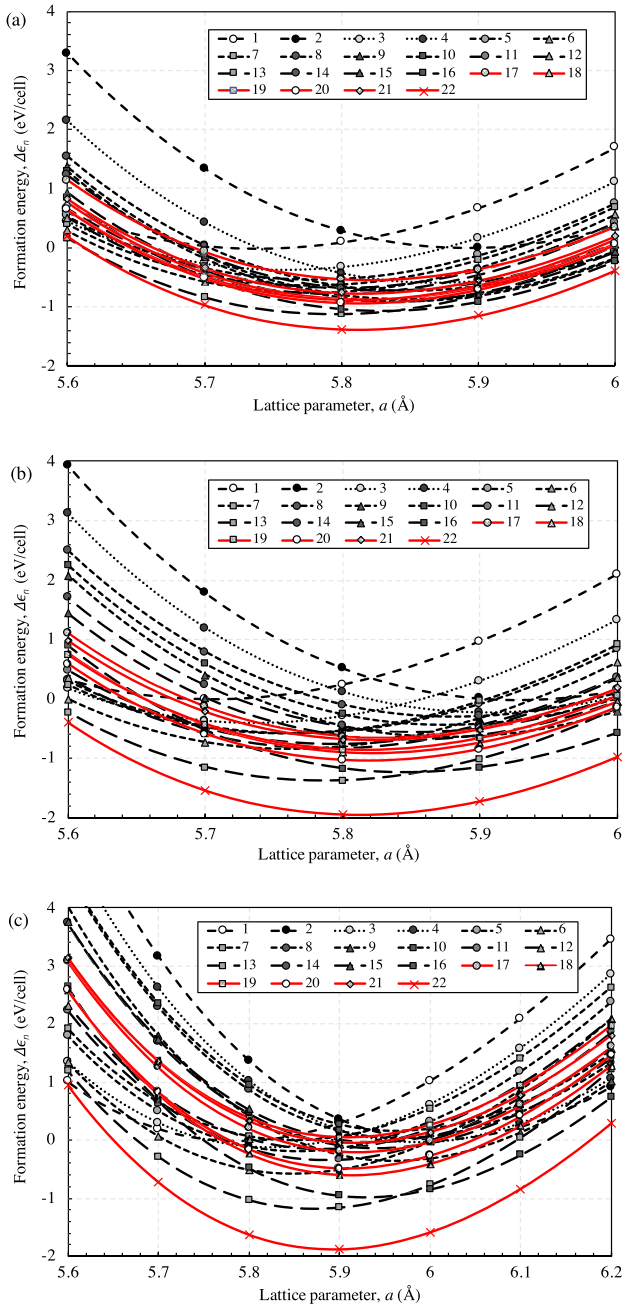

Figure 2. Calculated formation energies of the atomic configurations in table 1 for the (a) Fe–Al–Ti, (b) Co–Al–Ti, and (c) Ni–Al–Ti alloys. Here, the segregation limit connecting the minimum energies of the perfect B2 ordered phases, XAl and XTi, is considered as the reference energy.

The cubic interaction energies, $\epsilon_{ijklmnop}$ (or ϵ_n, where n represents one of the cubic configurations listed in table 1), are obtained from electronic band structure calculations utilizing the projector augmented-wave method [19], as implemented in the Vienna *Ab Initio* Simulation Package. A non-spin-polarization calculation is conducted utilizing the generalized gradient approximation of the Perdew–Burke–Ernzerhof [20] for the exchange-correlation functional. The supercells in these DFT calculations contain 16 atoms (the numbers of X, Al, and Ti atoms are 8, $8-N$, and N, respectively, where N takes an integer value from zero to eight) in the bcc structure, where X atoms are fixed on the γ-sublattice, and Al and Ti atoms are placed on the α- and β-sublattices, as shown in table 1. The plane wave cutoff energy is set to 400 eV and integration over the Brillouin zone is performed with $4 \times 4 \times 4$ k-points. The cubic interaction energies calculated at various volumes are fitted to the following Murnaghan equation of state [21]:

$$\epsilon_{ijklmnop}(V) = \epsilon_{ijklmnop}(V_0) + \frac{B_0 V}{B_0'(B_0'-1)}\left[B_0'\left(1-\frac{V_0}{V}\right)+\left(\frac{V_0}{V}\right)^{B_0'}-1\right], \quad (3)$$

where V_0 is an equilibrium volume at the ground state, B_0 is the bulk modulus at the equilibrium volume, and B_0' is the first derivative of the bulk modulus, B, with respect to pressure, P, which is evaluated at V_0 (i.e. $B_0' = (\partial B/\partial P)_{V_0}$).

The equilibrium state of a system at a finite temperature, T, is determined utilizing the grand potential, Ω. The grand potential is derived by performing a Legendre transformation on the Helmholtz free energy, F, in terms of point cluster probabilities, x_i $(= (x_i^\alpha + x_i^\beta)/2)$, as $\Omega = F - \sum_i \mu_i x_i$, where μ_i is the chemical potential of atomic species i. The equilibrium state is determined by imposing the following two conditions:

$$\left(\frac{\partial \Omega}{\partial w_{ijklmnop}^{\alpha\beta\alpha\beta\alpha\beta\alpha\beta}}\right)_{V,T} = 0 \quad (4)$$

and

$$\left(\frac{\partial \Omega}{\partial V}\right)_{T,x_i^\alpha,x_i^\beta,y_{ij}^{\alpha\beta},z_{ijkl}^{\alpha\beta\alpha\beta},w_{ijklmnop}^{\alpha\beta\alpha\beta\alpha\beta\alpha\beta}} = 0\,. \quad (5)$$

The minimization of the grand potential in terms of cluster probability (equation (4)) is performed utilizing the natural iteration method [22]. The phase boundary between $L2_1$ (or ordered) and B2 (or disordered) phases at each temperature is identified as the point at which their equilibrium grand potentials, $\Omega_{eq}(T)$, become identical (i.e. $\Omega_{eq}^{L2_1}(T) = \Omega_{eq}^{B2}(T)$).

3. Results and discussion

The calculated formation energies, $\Delta\epsilon_n$ (or $\Delta\epsilon_{ijklmnop}$), for each atomic configuration in X–Al–Ti (X: Fe, Co, and Ni) alloys in terms of lattice parameters, a $(= V^{\frac{1}{3}})$, are presented in figure 2, where the segregation limit connecting the minimum energies of the perfect B2 ordered phases, XAl and XTi, is considered as the reference energy. From figure 2, one can see that the $L2_1$ ordered structure has the minimum formation energy among all Fe–, Co–, and Ni–Al–Ti alloys. This indicates that the $L2_1$ ordered structure is the most stable phase at the ground state. The equilibrium lattice constant, a_0, and bulk modulus, B_0, of the perfect B2 and $L2_1$ ordered phases calculated utilizing the Murnaghan equation of state (equation (3)) are summarized in table 2. One can see that the calculated lattice constants are close to the experimental data, but there are nontrivial differences in the bulk moduli. The nontrivial differences in the bulk moduli of some ordered phases, such as FeAl (B2), CoTi (B2), and NiTi (B2), are consistent with the previous DFT calculations using full-potential

Table 2. Equilibrium lattice constant, a_0, and bulk modulus, B_0, of the perfect B2 and $L2_1$ ordered phases at the ground state evaluated utilizing the Murnaghan equation of state (equation (3)). Available experimental data are also provided (note that the experimental data were measured at ambient temperatures).

a_0 (Å)	Cal.	Exp.	Diff. (%)
FeAl (B2)	2.869	2.862 [26]	+0.24
FeTi (B2)	2.947	2.972 [27]	−0.85
Fe_2AlTi ($L2_1$)	5.812	5.882 [28]	−1.20
CoAl (B2)	2.851	2.861 [29]	−0.25
CoTi (B2)	2.965	2.995 [26]	−1.01
Co_2AlTi ($L2_1$)	5.812	5.85 [30]	−0.65
NiAl (B2)	2.894	2.886 [31]	+0.28
NiTi (B2)	3.006	3.012 [32]	−0.20
Ni_2AlTi ($L2_1$)	5.896	5.90 [33]	−0.40
B_0 (GPa)	Cal.	Exp.	Diff. (%)
FeAl (B2)	176.8	152 [34]	+16.3
FeTi (B2)	194.0	160.8 [35], 189 [36]	+17.1, +2.64
Fe_2AlTi ($L2_1$)	187.0	—	—
CoAl (B2)	175.7	162 [29]	+7.80
CoTi (B2)	181.0	154 [37]	+16.6
Co_2AlTi ($L2_1$)	183.3	—	—
NiAl (B2)	155.1	156 [31]	−0.58
NiTi (B2)	163.7	140.3 [38]	+14.3
Ni_2AlTi ($L2_1$)	162.7	—	—

linearized augmented plane waves method [23, 24] or full-potential linear muffin-tin orbitals method within the local density approximation [25].

The calculated phase diagrams in X–Al–Ti alloys at the pseudo-binary section, XAl–XTi, are presented in figure 3 with experimental results from previous studies [8–10]. One can see that there are only single-phase regions of B2 and $L2_1$ ordered phases in the Fe–Al–Ti alloy, whereas there are two-phase regions at low temperatures in both the Co–Al–Ti and Ni–Al–Ti alloys. These findings are consistent with the experimental results [8–10].

To clarify the reason for the absence of phase separation in the Fe–Al–Ti alloy, lattice misfits between the B2 and $L2_1$ ordered phases, $\delta_{B2/L2_1}$, at the ground state and the first- to third-nearest-neighbor effective pair interaction energies on the simple cubic lattice, $W^{(1,2,or3)}_{Al/Ti}$, were calculated for the X–Al–Ti alloys and are shown in table 3 and figure 4, respectively. A lattice misfit is defined as

$$\delta_{B2/L2_1} = \frac{|a_0^{L2_1} - a_0^{B2}|}{a_0^{B2}}, \tag{6}$$

where a_0^{B2} and $a_0^{L2_1}$ are the lattice constants of the B2 and $L2_1$ ordered phases at the ground state, respectively. The effective pair interaction energies are defined as $W^{(n)}_{Al/Ti} \equiv e^{(n)}_{AlAl} + e^{(n)}_{TiTi} - 2e^{(n)}_{AlTi}$, where $e^{(n)}_{AlAl}$, $e^{(n)}_{AlTi}$, and $e^{(n)}_{TiTi}$ are the nth-nearest-neighbor pair interaction energies of Al–Al, Al–Ti, and Ti–Ti pairs on the simple cubic lattice. The effective pair interaction energies can be utilized to evaluate the tendencies of ordering or phase separation in a system. When $W^{(n)}_{Al/Ti} > 0$ ($W^{(n)}_{Al/Ti} < 0$), the Al–Al and Ti–Ti pairs (Al–Ti and Ti–Al pairs) are preferred by the nth-nearest-neighbors. Their values can be extracted utilizing the cluster expansion method (CEM) [39] (details regarding the CEM can be found in appendix). From table 3 and figure 4, one can see that the lattice misfits for the Fe–Al–Ti alloy are much smaller than those for the Co– and Ni–Al–Ti alloys, and the first-nearest-neighbor interaction energy in the Fe–Al–Ti alloy is dominant compared to the second- and third-nearest-neighbor interaction energies. These results indicate that it is difficult to induce either mechanically or chemically driven phase separation in the Fe–Al–Ti alloy, meaning no phase separation behavior or two-phase regions could be produced.

In contrast, in the Ni–Al–Ti alloy, the lattice misfits are relatively large and the second-nearest-neighbor effective pair interaction shows a large negative value in table 3 and figure 4. These factors make the system mechanically unstable and chemically frustrating, resulting in phase separation. To confirm the mechanical instability of the Ni–Al–Ti alloy, P–V curves were calculated. One of the representative P–V curves for the Ni–Al–Ti alloy is presented in figure 5. This curve corresponds to $T = 1500$ K in the Al–rich side. One can see that the curve intersects the horizontal axis ($P = 0$) for three different lattice parameters. Among these intersections, the left and right intersection points satisfy the stability criteria, namely $\partial P/\partial V < 0$, and are considered to be stable phases (lattice constants are given at intersection points). In contrast, the middle intersection point is unstable based on the stability criteria, so it decomposes into the two stable phases. It was confirmed that the lattice parameters at the two intersections are the same as those of the B2 and $L2_1$ ordered phases, which were independently calculated in figure 3.

For the Co–Al–Ti alloy, the lattice misfit is as large as that for the Ni–Al–Ti alloy, but the second- and third-nearest-neighbor effective interaction energies are insignificant

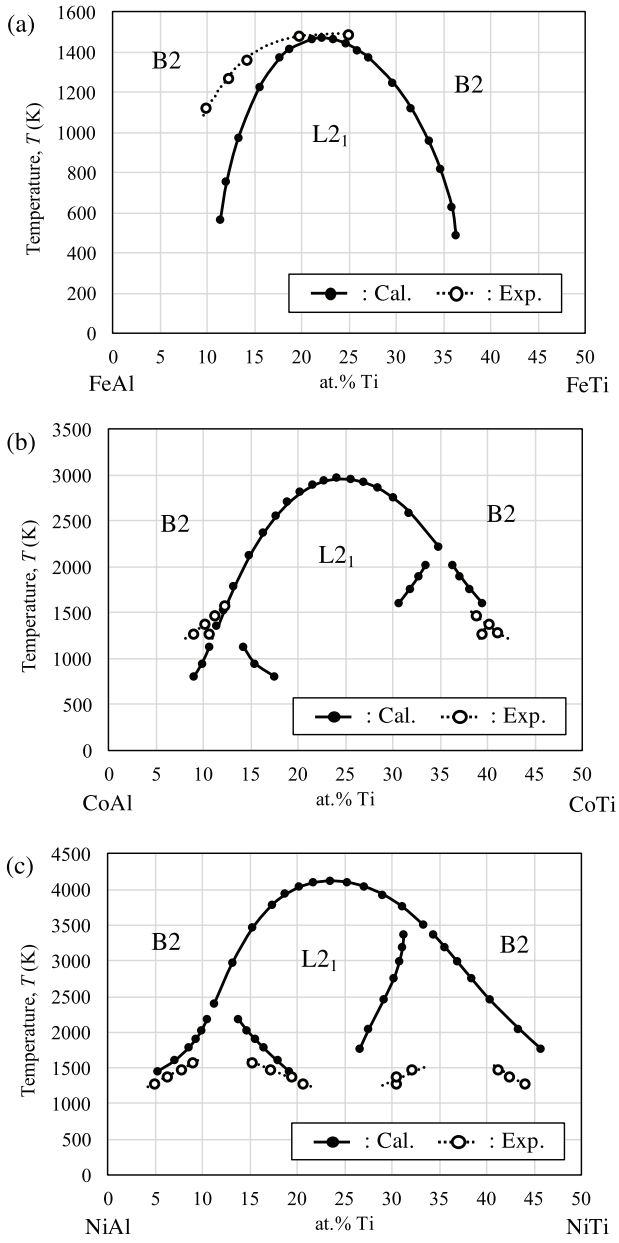

Figure 3. Phase boundaries between B2 and $L2_1$ ordered phases in the (a) Fe–Al–Ti, (b) Co–Al–Ti, and (c) Ni–Al–Ti alloys in the pseudo-binary section, XAl–XTi (X: Fe, Co, and Ni). The calculated results and experimental data [8–10] are shown as filled and open circles, respectively.

Table 3. Lattice misfits between B2 and $L2_1$ ordered structures at the ground state, which are calculated from table 2 and equation (6).

$\delta_{B2/L2_1}$	Fe–Al–Ti	Co–Al–Ti	Ni–Al–Ti
$\delta_{\mathrm{XAl/X2AlTi}}$	1.288%	1.922%	1.875%
$\delta_{\mathrm{XTi/X2AlTi}}$	1.398%	1.991%	1.942%

compared to the first-nearest-neighbor interaction energy. Therefore, it is considered that the phase separation behavior in the Co–Al–Ti alloy is solely caused by mechanical instability. This explains the smaller two-phase regions of B2 and

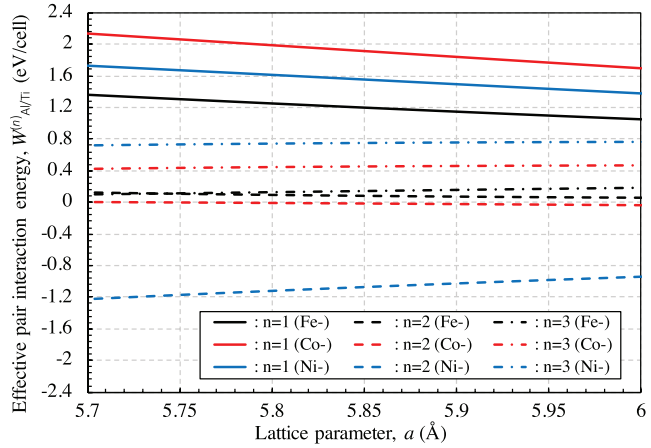

Figure 4. Effective pair interaction energies of the nth-nearest-neighbor pairs, $W^{(n)}_{\mathrm{Al/Ti}}$, calculated utilizing the CEM. The black, red, and blue lines represent the Fe–, Co–, and Ni–Al–Ti alloys, respectively. The first, second, and third effective interaction energies are shown in solid, broken, and broken-dotted lines, respectively.

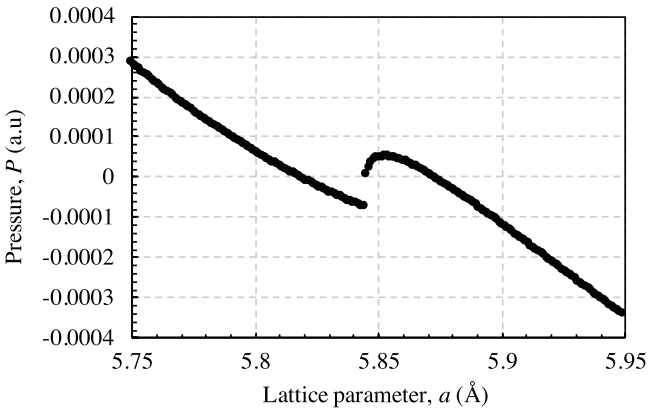

Figure 5. P–V curve on the Al–rich side of the Ni–Al–Ti alloy at $T = 1500$ K.

$L2_1$ ordered phases in the Co–Al–Ti alloy compared to those in the Ni–Al–Ti alloy (see figures 3(b) and (c)).

The large negative effective pair interaction energy of the second-nearest-neighbor pairs in the Ni–Al–Ti alloy is associated with the positive formation energies of certain atomic configurations (see figure 2(c)). In contrast, in the Fe– and Co–Al–Ti alloys, there are few configurations with positive formation energies (as shown in figures 2(a) and (b)), resulting in very small positive effective pair interaction energies in the Fe– and Co–Al–Ti alloys (see figure 4).

Note that there are some deviations in the calculated phase diagrams compared to the experimental results, such as a smaller B2 phase region in the Fe–Al–Ti alloy and overestimation of the two-phase regions on the Ti-rich side of the Co– and Ni–Al–Ti alloys. There are several possible reasons for these deviations, such as disregarding local atomic displacements, assuming that X atoms are located only at the γ-sublattice, and poor accuracy of the electronic band structure calculations. For a more reliable description of phase

Table A1. Twenty sub-clusters in the cubic cluster [16, 18]. Here, the cubic cluster is also shown. Each sub-cluster is numbered and its corresponding correlation function is provided. ξ_1, ξ_{2-4}, ξ_{5-7}, ξ_{8-13}, ξ_{14-16}, ξ_{17-19}, ξ_{20}, and ξ_{21} are the point, pair, triangle, four-body, five-body, six-body, seven-body, eight-body (or cubic) correlation functions, respectively.

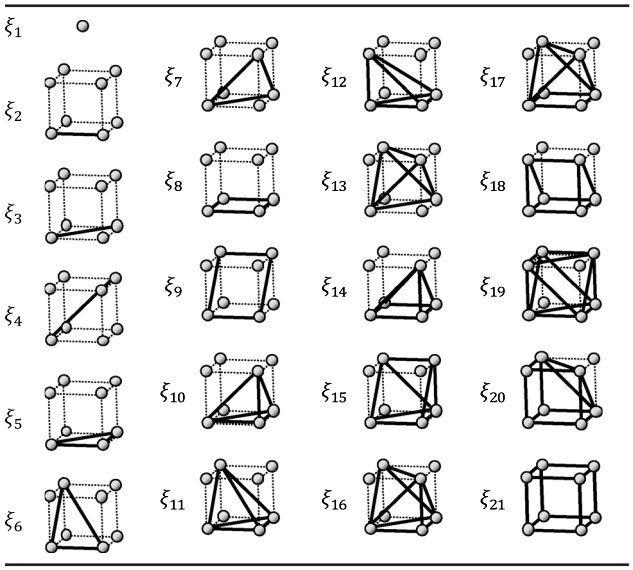

diagrams, it is necessary to consider these issues. Regarding the overestimation of two-phase regions in the Ti-rich side of the Co– and Ni–Al–Ti alloys, we believe that the accuracy of the interaction energies derived from the band structure calculations is the main problem. As shown in table 2, the deviations in the bulk modulus are much larger on the Ti-rich side than those in the Al-rich side.

Aside from the possible reasons mentioned above for the deviations from the experimental results in the calculated phase diagrams, there is a possibility that the approximation in the CVM itself causes some error. In the CVM, atomic correlations between different atomic species are truncated at a certain cluster size (which is a cubic cluster in this work), and higher order correlations are ignored. This problem may be circumvented by using a Monte Carlo method, in which all atomic correlations are automatically included. However, the semi-analytical feature of CVM facilitates easier numerical calculations and has some advantageous features to extract physical insight into the phase equilibria.

4. Conclusions

Phase diagrams of the X–Al–Ti (X: Fe, Co, and Ni) alloys (in the XAl–XTi pseudo-binary sections) were calculated utilizing the CVM based on interaction energies derived from electronic band structure calculations. The cubic approximation was adopted by assuming that interchange only occurs between the Al and Ti atoms on the α- and β-sublattices while X atoms are fixed on the γ-sublattice. Special attention was paid to the stability of B2 and $L2_1$ ordered phases, as well as the origin of phase separation behaviors in these alloy systems.

The calculated phase diagrams revealed that there are only single-phase regions in the Fe–Al–Ti alloy while there are two-phase regions of B2 and $L2_1$ ordered structures in both the Al- and Ti-rich sides in the Co– and Ni–Al–Ti alloys. Based on the lattice misfits between B2 and $L2_1$ phases and effective pair interaction energies, it was found that because neither mechanical instability nor chemical repulsions of unlike pairs are expected in the Fe–Al–Ti alloy, no phase separation behavior is observed. In contrast, mechanical instability and both mechanical instability and chemical repulsions are expected in the Co– and Ni–Al–Ti alloys, respectively. Therefore, the phase separation behaviors in the Co– and Ni–Al–Ti alloy systems are attributed to mechanical instability and a combination of mechanical instability and chemical repulsions, respectively.

It is believed that the presented formalism can be applied to other metallic alloy systems in which phase separations are observed. Clarifying the origins of phase separations in various alloy systems will facilitate the microstructure control of industrial materials in an effective manner.

Acknowledgment

We acknowledge Dr. K Sato from the Division of Materials and Manufacturing Science at the Graduate School of Engineering, Osaka University, Suita, Osaka for providing computational resources that contributed to the results reported within this paper.

Appendix. Cluster expansion method

The CEM [39] was employed to extract the effective pair interaction energies of the first-, second-, and third-nearest-neighbors between Al and Ti atoms on a simple cubic lattice. Based on the CEM, the formation energies, $\Delta E^{(n)}$ (corresponding to $\Delta\epsilon_n$ in this work, where n denotes one of the cubic configurations listed in table 1), are written as

$$\Delta E^{(n)} = \sum_m v_m \xi_m^{(n)} , \tag{A.1}$$

where v_m is the effective cluster interaction energy for a cluster m and $\xi_m^{(n)}$ is a correlation function. The cubic cluster is composed of 20 sub-clusters [16, 18] as shown in table A1. The correlation functions, $\xi_m^{(n)}$, are uniquely determined for each cubic configuration, n, utilizing the spin operator $\sigma(p)$, which takes on values of $+1$ or -1 depending on the existence of an Al or Ti atom at a lattice site p. Utilizing $\xi_m^{(n)}$ with the $\Delta E^{(n)}$ calculated from the band calculations (shown in figure 2), the effective cluster interaction energies, v_m, are determined as

$$v_m = \sum_n \left(\xi_m^{(n)}\right)^{-1} \Delta E^{(n)} , \tag{A.2}$$

where v_2, v_3, and v_4 correspond to the first-, second-, and third-nearest neighbor effective pair interaction energies. These values are related to $W_{\mathrm{Al/Ti}}^{(n)}$ as $W_{\mathrm{Al/Ti}}^{(1)} = 2v_2$, $W_{\mathrm{Al/Ti}}^{(2)} = 2v_3$, and $W_{\mathrm{Al/Ti}}^{(3)} = 2v_4$.

Note that based on the use of effective cluster interaction energies, v_m, and correlation functions, ξ_m, the total energy of a system can be expressed as

$$E = \sum_m v_m \xi_m \ . \tag{A.3}$$

Here, the superscripts of the sublattices (α and β) are omitted. Equation (A.3) corresponds to equation (2) if all multi-body effective interaction energies up to the cubic level are considered. The correlation functions and cluster probabilities are directly correlated, as demonstrated in [40]. One of the biggest advantages of utilizing correlation functions instead of cluster probabilities is that it can significantly reduce the number of variables necessary for calculations. Although we did not encounter any computational issues related to large numbers of variables in this work, for more demanding calculations (such as the continuous-displacement CVM [41] in a three-dimensional lattice), the replacement of cluster probabilities with correlation functions would be required.

ORCID iDs

Ryo Yamada https://orcid.org/0000-0002-3064-0186

References

[1] Haasen P 1978 *Physical Metallurgy* (Cambridge: Cambridge University Press)

[2] Girifalco L A 2003 *Statistical Mechanics of Solids* vol 58 (Oxford: Oxford University Press)

[3] Mohri T and Chen Y 2004 First-principles calculation of $L1_0$-disorder phase boundary in Fe–Pd system *Mater. Trans.* **45** 1478–84

[4] Ino H 1978 A pairwise interaction model for decomposition and ordering processes in BCC binary alloys and its application to the Fe–Be system *Acta Metall.* **26** 827–34

[5] Allen S M and Cahn J W 1976 Mechanisms of phase transformations within the miscibility gap of Fe-rich Fe–Al alloys *Acta Metall.* **24** 425–37

[6] Soffa W A and Laughlin D E 1989 Decomposition and ordering processes involving thermodynamically first-order order→disorder transformations *Acta Metall.* **37** 3019–28

[7] Inden G 1974 Ordering and segregation reactions in BCC binary alloys *Acta Metall.* **22** 945–51

[8] Kainuma R, Urushiyama K, Ishikawa K, Jia C C, Ohnuma I and Ishida K 1997 Ordering and phase separation in bcc aluminides of the Ni–Fe–Al–Ti system *Mater. Sci. Eng.* A **239** 235–44

[9] Ishikawa K, Mitsui H, Ohnuma I, Kainuma R, Aoki K and Ishida K 2002 Ordering and phase separation of BCC aluminides in (Ni, Co)–Al–Ti system *Mater. Sci. Eng.* A **329** 276–81

[10] Ishikawa K, Kainuma R, Ohnuma I, Aoki K and Ishida K 2002 Phase stability of the X_2AlTi (X: Fe, Co, Ni and Cu) Heusler and B2-type intermetallic compounds *Acta Mater.* **50** 2233–43

[11] Oh-ishi K, Horita Z and Nemoto M 1997 Phase separation and lattice misfit in NiAl(β_1)–Ni_2AlTi(H)–NiTi(β_2) system *Mater. Trans. JIM* **38** 99–106

[12] Enomoto M and Kumeta T 1997 Analysis of the β'Ni_2TiAl/β NiTi equilibrium in Ni–Ti–Al alloys by the cluster variation method *Intermetallics* **5** 103–9

[13] Kikuchi R 1951 A theory of cooperative phenomena *Phys. Rev.* **81** 988–1003

[14] Mohri T, Chen Y and Kiyokane N 2013 First-principles cluster variation calculations of tetragonal-cubic transition in ZrO_2 *J. Alloys Compd.* **577** S123–6

[15] Morán-López J L and Sánchez J M 2012 *Theory and Applications of the Cluster Variation and Path Probability Methods* (Berlin: Springer)

[16] Kiyokane N 2012 Model calculations of replacive- and displacive-type phase transformations using the cluster variation method (in Japanese) *PhD Thesis* Hokkaido University

[17] Yamada R and Mohri T 2019 Application of cluster variation and path probability methods to the tetragonal–cubic phase transition in ZrO_2 *J. Phys. Soc. Japan* **88** 074005

[18] Kiyokane N and Mohri T 2010 Order of phase transition on a simple cubic lattice determined by cluster variation method *Mater. Trans.* **51** 463–8

[19] Kresse G and Furthmüller J 1996 Efficiency of *ab initio* total energy calculations for metals and semiconductors using a plane-wave basis set *Comput. Mater. Sci.* **6** 15–50

[20] Perdew J P, Burke K and Ernzerhof M 1996 Generalized gradient approximation made simple *Phys. Rev. Lett.* **77** 3865–8

[21] Tyuterev V G and Vast N 2006 Murnaghan's equation of state for the electronic ground state energy *Comput. Mater. Sci.* **38** 350–3

[22] Kikuchi R 1974 Superposition approximation and natural iteration calculation in cluster-variation method *J. Chem. Phys.* **60** 1071–80

[23] Bihlmayer G, Eibler R and Neckel A 1994 Elastic properties of b2-niti and b2-pdti *Phys. Rev.* B **50** 13113

[24] Cheng D, Zhao S, Wang S and Ye H 2001 First-principles study of the elastic properties and electronic structure of NiTi, CoTi and FeTi *Phil. Mag.* A **81** 1625–32

[25] Nguyen-Manh D and Pettifor D G 1999 Electronic structure, phase stability and elastic moduli of ab transition metal aluminides *Intermetallics* **7** 1095–106

[26] Villars P and Calvert L D 1986 *Pearson's Handbook of Crystal Data for Intermetallic Phases* vol 1–3 (Metals Park, OH: American Society for Metals)

[27] Van der Kraan A M and Buschow K H J 1986 The 57Fe Mössbauer isomer shift in intermetallic compounds of iron *Physica* B + C **138** 55–62

[28] Okpalugo D E, Booth J G and Faunce C A 1985 Onset of ferromagnetism in 3d-substituted FeAl alloys. I. Ti, V and Cr substitutions *J. Phys. F: Met. Phys.* **15** 681

[29] Ogut S and Rabe K M 1994 *Ab initio* pseudopotential calculations for aluminum-rich cobalt compounds *Phys. Rev.* B **50** 2075

[30] Carbonari A W, Saxena R N, Pendl W Jr, Mestnik Filho J, Attili R N, Olzon-Dionysio M and De Souza S D 1996 Magnetic hyperfine field in the Heusler alloys Co2YZ (Y = V, Nb, Ta, Cr; Z = Al, Ga) *J. Magn. Magn. Mater.* **163** 313–21

[31] Otto J W, Vassiliou J K and Frommeyer G 1997 Equation of state of polycrystalline Ni_50Al_50 *J. Mater. Res.* **12** 3106–8

[32] Matsumoto H and Ishiguro H 1989 Lattice constant, elastic modulus and electrical resistivity of $Ni_{50}Ti_{50-x}al_x$ *J. Less-Common Met.* **153** 57–63

[33] Oh-Ishi K, Horita Z and Nemoto M 1997 Microstructure and strength of B2-ordered nial containing l21-ni2alhf precipitates *Mater. Sci. Eng.* A **239** 472–8

[34] Zhang X D and Sauthoff G 1995 Analysis of relationships between cohesive energy, elastic moduli and lattice parameter of some high temperature intermetallics *Intermetallics* **3** 137–40
[35] Liebertz J, Stähr S and Haussühl S 1980 Growth and properties of single crystals of FeTi *Krist. Tech.* **15** 1257–60
[36] Buchenau U, Schober H R, Welter J M, Arnold G and Wagner R 1983 Lattice dynamics of $Fe_{0.5}$ $Ti_{0.5}$ *Phys. Rev.* B **27** 955
[37] Yasuda H, Takasugi T and Koiwa M 1991 Elastic constants of Co_3Ti and CoTi intermetallic compounds *Mater. Trans. JIM* **32** 48–51
[38] Mercier O, Melton K N, Gremaud G and Hägi J 1980 Single-crystal elastic constants of the equiatomic NiTi alloy near the martensitic transformation *J. Appl. Phys.* **51** 1833–4
[39] Connolly J W D and Williams A R 1983 Density-functional theory applied to phase transformations in transition-metal alloys *Phys. Rev.* B **27** 5169
[40] Mohri T 2013 Cluster variation method *JOM* **65** 1510–22
[41] Kikuchi R 1998 Space is continuous–continuous-displacement treatment of phase-separating diagrams *J. Phase Equilib.* **19** 412–21